



Green bionanocomposite based on kefiran and cellulose nanocrystals produced from beer industrial residues



Iman Shahabi-Ghahfarrokhi^{a,*}, Faramarz Khodaiyan^b, Mohammad Mousavi^b, Hossein Yousefi^c

^a Department of Food Science and Technology, Faculty of Agriculture, University of Zanjan, 45371-38791 Zanjan, Iran

^b Department of Food Science and Engineering, Campus of Agriculture and Natural Resources, University of Tehran, P.O. Box 4111, Karaj, Iran

^c Department of Wood Engineering and Technology, Gorgan University of Agricultural Sciences and Natural Resources, 4913815739 Gorgan, Iran

ARTICLE INFO

Article history:

Received 9 January 2015

Received in revised form 5 February 2015

Accepted 24 February 2015

Available online 20 March 2015

Keywords:

Kefiran

Nanocellulose

Biopolymer

ABSTRACT

Environmental concern about synthetic polymers and nanoparticles bring about development of the green bionanocomposite. Nanocellulose (NC) as safe nanofiller was prepared from beer industrial residues by acid hydrolysis in this study. ATR–FTIR spectrum showed no change in chemical structure of kefiran and NC after mixing. However, mechanical, visual, and WVP properties of kefiran/NC films improved with NC, but thermal properties and water sensitivity of them declined, simultaneously.

© 2015 Elsevier B.V. All rights reserved.

1. Introduction

Environmental concerns, finitude of petroleum resources, and increasing the oil price during the recent years have been three main reasons for paying considerable attention to biodegradable polymers from renewable resources. Hence, now there is an increasingly growing attention to biodegradable polymer as a gas and moisture barrier to increasing foods shelf-life. Although biodegradable polymers have several advantages, there are some restrictions in their application, e.g. low mechanical and weak moisture barrier properties [1,2].

Kefiran, as a microbial polysaccharide, produced during kefir production, has attracted much attention as an interesting biopolymer over the recent years [1–5]. This biopolymer is extracted from kefir grain as a byproduct of kefir production process. Kefir has functional properties such as antimutagenic and antimicrobial activities that can be affected by kefiran [6]. Previous researches showed that the mechanical properties and the water vapor permeability (WVP) of kefiran film were comparable with some synthetic polymers [3], but our results showed that kefiran had considerable mechanical and visual properties. However, the WVP of kefiran is not as good

as synthetic polymers; consequently, it needs some modifications [2,7].

Different nanoparticles have been mixed with biopolymers to give them more strength and barrier properties [1,2,8,9], but there are some concerns about ecological pollution and toxic properties of nanoparticles [10]. In contrast, green nanoparticles like nanocellulose (NC) are safe and biodegradable reinforcing agents [11,12].

Acid hydrolysis is the most frequently used method to prepare cellulose nanostructure in which rod-like cellulose nanocrystals are isolated [13]. If the hydrolysis intensity is high enough, the aspect ratio of cellulose nanowhiskers decreases to less than two [12]. Such produced cellulose nanocrystals are commonly named spherical cellulose nanocrystals, which were prepared in our previous study using beer industrial residues (BIR) as raw material [13]. The cellulose nanocrystal is hereafter called nanocellulose (NC).

The main scope of the current research is to reinforce kefiran biopolymer by produced NC using BIR. Moreover, the physical, thermal, mechanical and chemical properties of kefiran/NC nanocomposite are characterized and discussed.

2. Materials and methods

2.1. Material

BIR was collected from Behnoosh malt industrial Co., Iran. The analytical grade chemicals, including sodium hydroxide (NaOH), potassium hydroxide (KOH), calcium chloride (CaCl₂), sodium

* Corresponding author. Tel.: +98 9132804889; fax: +98 2433052348.

E-mail addresses: i.shahabi@znu.zc.ir, i.shahabi@yahoo.com (I. Shahabi-Ghahfarrokhi).

chloride (NaCl), acetic acid (CH_3COOH), and hydrochloric acid (HCl) were purchased from Dr. Mojallai Co., Iran. Sodium chlorite (NaClO_2) was also provided from Fluka Chemical Co., Germany.

2.2. Preparation of NC

NC was prepared according to our previous study [13]. BIR (1:10) was boiled for 1 h and dried at 105°C . The dried BIR (1:10) was then soaked in NaOH (2%) overnight. The soaked BIR was washed with water and then was treated by 12% NaOH at 121°C for 45 min (three times) to produce BIR pulp. The BIR pulp was washed and subsequently dried at 105°C . To remove residual lignin, the pulp slurry (1:20) was treated twice by a solution containing 3% NaClO_2 and 1.5% CH_3COOH at 75°C for 1 h. To remove hemicelluloses and residual starch, the treated pulp was soaked in 3% KOH solution overnight, followed by treating at 80°C for 1 h. The pulp was further bleached using 3% NaClO_2 and 1.5% CH_3COOH at 75°C for 1 h. Finally, the purified cellulose of BIR was dried at 105°C [13].

The slurry of purified BIR cellulose (1:10) was hydrolyzed by 10% HCl at 80°C for 4 h. The hydrolyzed cellulose was washed 3 times by centrifugation (Mikro 200, Hettich, Germany) at 6000 rpm, 4°C for 30 min. Next, for removing residual acid and neutralizing pH, dialysis tube (Sigma Aldrich, Germany) soaked in distilled water was used. To disperse coagulated neutralized cellulose particles, ultrasonic treatment (Hielscher UP200S, Germany) for 15 min resulted in NC. The average diameter of NC was 97 ± 18 nm [13].

2.3. Kefiran purification

Kefir grains were dissolved in boiling water (1:10) for 30 min. After the first centrifugation at $10,000 \times g$ for 30 min, all of the undissolved portions of grain were almost decanted. Then, polysaccharides were precipitated by mixing with chilled ethanol (1:1) at -18°C overnight. Purification procedure was followed by centrifuging at $10,000 \times g$ for 30 min at 4°C and three times washing with water for removing water solvable impurities [2]. The white precipitated polysaccharide is hereafter called kefir. The total polysaccharide content of kefir was 92% according to the phenol sulfuric method [14].

2.4. Film preparation

The aqueous solution of 2 wt% kefir was prepared and 40 wt% (dry base) glycerol as plasticizer was added to it. On the other hand, NC was dispersed in distilled water by sonication for 30 min at room temperature. Different concentrations of NC dispersion (1, 2 and 3 wt% (dry base)) were added to the aqueous solution of kefir and mixed for 10 min. After degassing, the film forming solutions were casted by pouring the mixture onto Teflon plates and dried at 25°C in oven and room relative humidity. The dried films were peeled off the casting surface. All the film specimens were conditioned inside desiccators containing saturated calcium nitrite (Merck Co., Germany) solution to ensure a relative humidity of 55% at $25 \pm 1^\circ\text{C}$ for 48 h.

2.5. Microstructure

Microstructural analysis of the cross-sections and surface area of the dried films was conducted by SEM (CamScan MV2300, Canada). The films specimens were sputtered with gold using a KYKY-SBC-12 sputter coater (KYKY, China). All cross-sections and surface area specimens were examined using an accelerating voltage of 19.0 kV.

An atomic-force microscope (AFM, DualscopeC26, DME, Denmark) was used to take micrographs of the NC. The specimen

was placed onto freshly cleaved mica and left to dry at room temperature prior to scanning.

2.6. Measurements

2.6.1. Thickness

The thickness of specimens was measured by a hand-held micrometer with an accuracy of 0.01 mm at 13 random positions for each film.

2.6.2. Moisture content

The moisture content (MC) of the specimens was determined (three replicates) by measuring the weight loss of films before and after drying in a laboratory oven (Shimaz Co., Iran) at $105 \pm 1^\circ\text{C}$ until constant weight.

2.6.3. Moisture absorption

Moisture absorption (MA) was measured according to the method of Almasi et al. [8]. In brief, the dried sheets of $20 \times 20 \text{ mm}^2$ were first conditioned at 0% RH (prepared by dried calcium sulphate) for 24 h. After weighing, they were conditioned in a desiccator containing saturated calcium nitrite solution at 25°C to ensure a relative humidity of 55%. The specimen was weighed at desired intervals until the equilibrium state was reached. The moisture absorption of the specimen was calculated with Eq. (1):

$$\text{MA} = \frac{W_e - W_0}{W_0} \times 100 \quad (1)$$

where W_e and W_0 are the weights of specimen after equilibration at 55% RH and the initial weight of the specimen, respectively. All measurements were performed in three replicates.

2.6.4. Solubility

Solubility in water (SW) was defined as the ratio of the water-soluble dry matter of film that is dissolved after immersion in distilled water [4]. A $20 \times 20 \text{ mm}^2$ specimen was cut from each film, dried at $105 \pm 1^\circ\text{C}$ to constant weight in a laboratory oven (Shimaz, Iran), and weighed to determine the initial dry weight (m_1). The solubility in water of the specimen was measured from immersion assays in 50 ml of distilled water with periodic stirring for 6 h at 25°C . After that period, the remaining pieces of films were taken out and dried at $105 \pm 1^\circ\text{C}$ until constant weight (m_2). SW of the specimens were calculated using Eq. (2):

$$\text{SW} = \frac{m_1 - m_2}{m_1} \times 100 \quad (2)$$

2.6.5. Color

Film color was determined using a colorimeter (Labscan XE, Hunterlab, USA). Film specimens were placed on a white standard plate and the lightness (L) and chromaticity parameters a (red–green) and b (yellow–blue) were measured. All the colors can be explained by L values ranging from 0 (black) to 100 (white); minus values of a (greenness) to its positive value (redness); and minus values of b (blueness) to its positive value (yellowness). All measurements were performed in 5 replicates. Total color difference (ΔE) and whiteness index (WI) were calculated using Eqs. (3) and (4) [4]:

$$\Delta E = \sqrt{(L^* - L)^2 + (a^* - a)^2 + (b^* - b)^2} \quad (3)$$

where L^* , a^* , and b^* are the color parameter values of standard ($L^* = 93.7$, $a^* = -1.13$ and $b^* = 1.24$) and L , a , and b are the color parameter values of the specimen:

$$\text{WI} = 100 - \sqrt{(100 - L)^2 + a^2 + b^2} \quad (4)$$

2.6.6. WVP

The water vapor permeability (WVP) of films was measured gravimetrically according to ASTM E96 standard [15] and corrected for the stagnant air gap inside test cups [16]. Special glass vials with the diameter of 12.62 mm and the volume of 10 ml were used as test cups. The area of the vial mouth and depth were $1.25 \times 10^{-4} \text{ m}^2$ and 43 mm, respectively. The vial containing calcium chloride desiccant (0% RH, assay cup) or nothing (control cup), were covered with film specimens and sealed to the vial mouths using parafin. Each vial was placed in a desiccator and maintained at 75% RH with a saturated solution of sodium chloride (Dr Mojalali Co., Iran). The difference in RH corresponds to a driving force of 1753.55 Pa, expressed as water vapor partial pressure. After the films were mounted, the weight gain of the whole assembly was periodically recorded (with an accuracy of 0.0001 g) every 1 h during the first ten hours and finally after 25 h. The slope (S) of the weight-vs.-time plot ($R^2 \geq 0.986$) was divided by the effective film area (A) to obtain the water vapor transmission rate (WVTR) Eq. (5). This was multiplied by the thickness of the film and divided by the pressure difference between the inner and outer surfaces to obtain the WVP Eq. (6)

$$\text{WVTR} = \frac{S}{A} \quad (5)$$

$$\text{WVP} = \frac{\text{WVTR} \times X}{\Delta P} \quad (6)$$

where X is the average film thickness (m) and ΔP is the driving force (1753.55 Pa).

2.7. Mechanical properties

Tensile strength (TS), elongation at break (EB), tensile energy to break (TEB), and Young's modulus (YM) were evaluated by Machine M350-10CT (Testometric Co., Ltd., Rochdale, Lancs., England) according to ASTM standard method D882-02 [17]. Films were cut in rectangular ribbon of 100 mm long by 10 mm wide. All specimens were conditioned at $50 \pm 5\%$ relative humidity for 48 h in a desiccator containing saturated calcium nitrate solution. The ribbons were fixed with an initial grip separation of 50 mm and stretched at a cross-head speed of 10 mm/min. Three replicates were run for each film specimen. TS, EB and TEB were calculated by Eqs. (7)–(9):

$$\text{TS} = \frac{F_{\max}}{A_{\min}} \quad (7)$$

$$\text{EB} = \frac{L_{\max}}{L_0} \times 100 \quad (8)$$

$$\text{TEB} = \frac{A_{\text{Stress-Strain}}}{V} \quad (9)$$

where F_{\max} is maximum load, A_{\min} is minimum cross section area, L_{\max} is extension at the moment of rupture, L_0 is initial length of specimen, $A_{\text{Stress-Strain}}$ is area under stress-strain curve and V is the volume of original gage region.

YM was calculated by drawing a tangent to the initial linear portion of the force-extension curve, selecting any point on this tangent and dividing the tensile stress by the corresponding strain.

2.8. FTIR

The IR spectrum of BIR pulp and NC were determined using a Fourier transform infra-red (FTIR) spectrometer (IRPrestige-21, Shimadzu, Japan). The specimens were ground with KBr powder and pressed into pellets for FTIR measurement in the wave-number range of $4000\text{--}400 \text{ cm}^{-1}$ by accumulation of 40 scans at a resolution of 4 cm^{-1} .

Attenuated total reflectance/Fourier transform infra-red (ATR/FTIR) spectra of the films were acquired using a FTIR spectrometer (IRPrestige-21, Shimadzu, Japan) and ATR accessory with ZnSe crystal plate and pressure-arm (Perkine Elmer Inc, USA). The film specimens were deposited on the ATR accessories. Spectra were obtained in the $600\text{--}4000 \text{ cm}^{-1}$ range by accumulation of 40 scans at 1.0 cm^{-1} resolution.

2.9. Differential scanning calorimetry (DSC)

The thermal properties of the films were carried out using DSC equipment (Metler Toledo, USA) according to ASTM standard method D 3418-08 [18]. Approximately 6 mg film specimen was cut and placed into a pan of DSC equipment. The specimens were then scanned at a heating rate of $10^\circ\text{C}/\text{min}$ between temperatures ranging from -50 to 160°C . Nitrogen was used as the purge gas at a flow rate of 20 ml/min. The glass transition temperatures (T_g) of the different films were determined from resulting thermograms as the midpoint temperature of a step-down shift in baseline, due to the discontinuity of the specific heat of the specimen. The melting point (T_m) was calculated as the temperature where the peak of the endotherm occurs. All these properties were determined in duplicates and the results were averaged.

2.10. Statistical analysis

Statistics on a completely randomized design were performed with the analysis of variance (ANOVA) procedure using SPSS software (Version 11.5; SPSS Inc., USA). Duncan's multiple range tests were used to compare the differences among mean values of film specimens' properties at the level of 0.05.



Fig. 1. Kefiran/NC nanocomposites with different NC content.

3. Results and discussion

3.1. Microstructure

Kefiran and NC are both polysaccharide and hydrophilic and have good compatibility; hence, the NC nanostructures were simply and properly distributed in the matrix of kefiran during nanocomposite fabrication and a homogeneity was observed at macroscale of nanocomposite structure (Fig. 1).

Fig. 2a shows the AFM micrograph of NC used as a reinforcing agent in the current study. As shown in Fig. 2b–e the heterogeneity of the cross-section of film specimens increased with increasing NC content. Similar changes were also observed in the previous studies in the cross-section of cellulose nanocomposites [11,19]. The high surface energy of nanoparticles [20] caused coagulation of NCs in polymer matrix with increasing NC content in the nanocomposite, especially in kefiran/NC 3% (Fig. 2e).

3.2. FTIR

The FTIR spectra of purified BIR fiber and NC are shown in Fig. 3a. FTIR spectra of carbohydrate are approximately as the same. The broad spectrum from $3700\text{--}3100\text{ cm}^{-1}$ contains the fundamental stretching modes of hydroxyl groups (O–H) due to carbohydrates and vibrations of the hydrogen bonded hydroxyl groups [21–24]. The spectrum from $3000\text{ to }2800\text{ cm}^{-1}$ could be attributed to the symmetric and anti-symmetric stretching modes of C–H in methyl (CH_3) and methylene (CH_2) functional groups [23,24]. The peaks at 2902 cm^{-1} were due to the aliphatic saturated C–H stretching vibration in carbohydrates [21]. The peak around 1640 cm^{-1} was assigned to C=C stretching band and associated with the adsorbed water [22,24]. The spectrum from $1500\text{ to }1300\text{ cm}^{-1}$ was attributed to the C–H bending bands [24]. After acid hydrolysis, the peak at 1325 cm^{-1} was eliminated in NCs. The peak at 1325 cm^{-1} was attributed to S ring (CH_2 rocking at C6 in cellulose) [23]. It seems the developed hydrogen-bonding network in

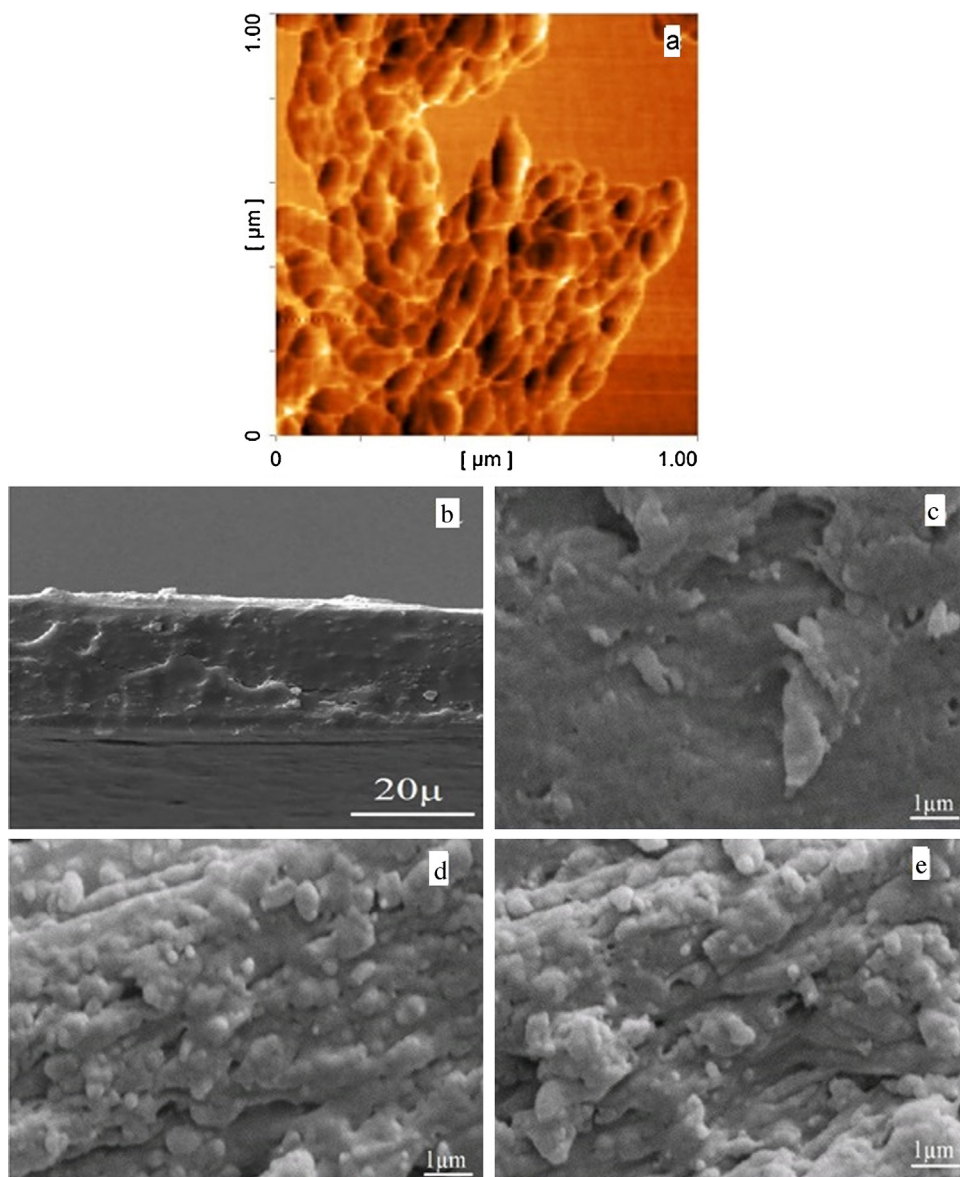


Fig. 2. (a) AFM micrograph of NC. SEM micrograph of the cross-section of specimens: (b) kefiran, (c) kefiran/NC 1%, (d) kefiran/NC 2%, and (e) kefiran/NC 3%.

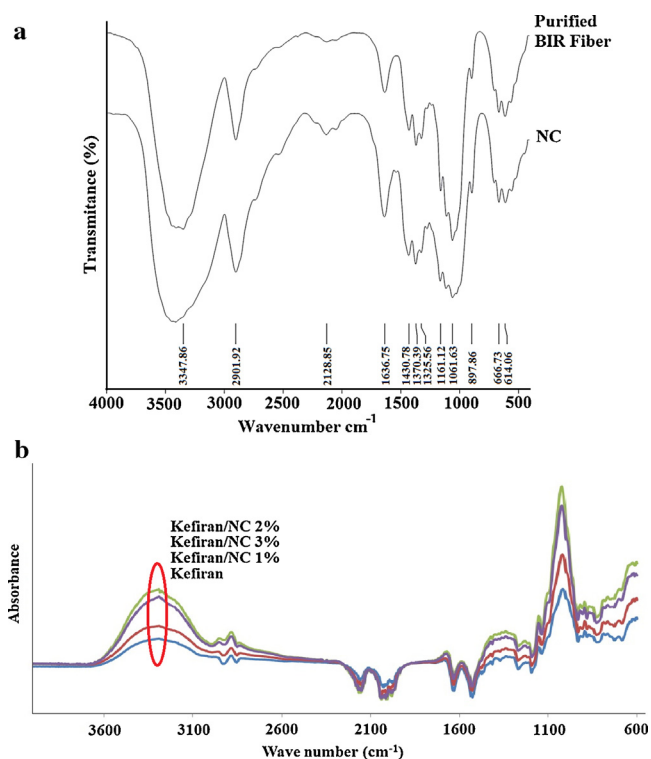


Fig. 3. (a) FTIR spectra of BIR pulp and NC. (b) ATR-FTIR spectra of kefir and kefir/NC composites with different NC content.

crystalline structure of NCs decreased the rocking movement of CH_2 . $1200\text{--}950\text{ cm}^{-1}$ a broad and intense band which holds the peaks was mainly assigned to stretching modes of carbohydrate rings and side group (C--O--C , C--OH , C--H) [23–25]. The peak at 896 cm^{-1} indicated the typical structure of cellulose (due to β -glycosidic linkages of glucose ring of cellulose) and C--H rocking vibrations of cellulose [21,22].

The absence of change in ATR-FTIR spectra of kefir and kefir/NC bionanocomposites (Fig. 3b) was attributed to the absence of change in the chemical bound between kefir and NC. However, Grande et al., observed some changes in FTIR spectra of starch/nano bacterial cellulose at the wavenumber $1100\text{--}950\text{ cm}^{-1}$ [26]. It seems that these changes in FTIR spectra depend on polymer type and the preparation method of NC.

4. Physical properties

4.1. Sensitivity to water

The physical properties of kefir and kefir/NC nanocomposite films are shown in Table 1. MC and MA of kefir/NC nanocomposite films increased with increasing NC content. Kaushik et al. believed that good interfacial adhesion between filler and matrix improved water resistance and mechanical properties of starch/NC bionanocomposites [19]. Furthermore, they showed

the increase of NC content in thermoplastic starch/NC composite films increased MA and MC in the film specimens [19]. This result is also consistent with ours. However, Soykeabkaew et al., showed that increasing NC content in starch base biocomposite decreased MA and MC of the film specimens [27]. It seems that NC preparation method, NC content and polymer type were effective parameters in sensitivity of bionanocomposite to water [19,27]. In addition, the plasticizing effects of residual mono and disaccharides, produced by acidic hydrolysis [25], and hydrophilic substituents of NC [19] intensified the MA and MC values of kefir/NC composites film. This caused enhancing the sensitivity of specimens to water.

As presented in Table 1, the SW of kefir/NC nanocomposites decreased as the result of using NC at the loading fraction of 1 wt%. However, increasing NC content intensified the SW of kefir/NC films. It seems hydrophilic properties and heterogenous distribution of NC in polymer matrix in high NC content (Fig. 2c–e) attenuated the stability of polymer structure [19] and increased solubility of polymer in water.

4.1.1. WVP

As shown in Table 1, WVP of kefir/NC nanocomposites significantly decreased with increasing NC content up to 2 wt%. The previous study showed that increasing NC content in polymer matrix decreased WVP of nanocomposite with increasing tortuosity of the polymer and cohesion of polymer matrix and nanofiller [28]. The WVP values of kefir/NC composite increased in nanocomposite containing 3 wt% NC. As shown in Fig. 2, increasing NC led to heterogeneous distribution of NC in polymer matrix, disruption of kefir matrix, and an increase of WVP in the film specimens.

4.1.2. Visual properties

Table 2 showed visual properties of kefir and kefir/NC composite. Lightness factor (L) of film specimens increased with increasing NC content up to 2 wt% and decreased in the film containing 3 wt% NC. Redness-greenness factor (a) of all kefir/NC composites showed a significant difference from kefir film specimens. Yellowness-blueness factor (b) increased after increasing NC content. However, there was no significant difference between ΔE value of kefir and that of kefir/NC composite films. Furthermore, there was no significant difference between WI value of kefir and that of kefir/NC composite films up to NC loading fraction of 2 wt%, but the WI value decreased at higher NC loading fraction (3 wt%) significantly.

4.2. Mechanical properties

Stress vs. strain curve of kefir and kefir/NC composites are shown in Fig. 4. The curves reported in Fig. 4 show an improvement of the mechanical strain with the increase of NC content.

Mechanical properties of kefir and kefir/NC composite are shown in Table 3. There was not a significant difference between TS value of kefir and that of kefir/NC nanocomposite, but kefir/1% NC specimens showed the maximum TS value. As shown in Fig. 2d and e, the coagulation of NC at higher loading fraction destroyed the structural integrity of polymer matrix and reduced

Table 1
Physical properties and WVP of kefir and kefir/NC composites with different NC content.

Nanocellulose content (%)	Moisture content (%)	Moisture absorption (%)	Solubility in water (%)	WVP ($\times 10^{-10}\text{ g m}^{-1}\text{ s}^{-1}\text{ Pa}^{-1}$)
0	$13.81 \pm 2.82\text{b}$	$9.34 \pm 0.34\text{b}$	$32.47 \pm 1.64\text{b}$	$2.19 \pm 0.00\text{a}$
1	$15.06 \pm 2.60\text{b}$	$9.68 \pm 1.84\text{ab}$	$19.82 \pm 2.47\text{c}$	$1.73 \pm 0.15\text{b}$
2	$17.89 \pm 0.40\text{ab}$	$10.85 \pm 0.79\text{ab}$	$31.25 \pm 3.61\text{b}$	$1.83 \pm 0.16\text{b}$
3	$21.78 \pm 2.61\text{a}$	$12.53 \pm 2.29\text{a}$	$52.68 \pm 4.02\text{a}$	$2.37 \pm 0.16\text{a}$

Means within each column with same letters are not significantly different ($P < 0.05$). Data are mean \pm SD.

Table 2

Visual properties of kefir and kefir/NC composites.

Nanocellulose content (%)	<i>L</i>	<i>a</i>	<i>b</i>	ΔE	WI
0	89.64 ± 0.74bc	0.00 ± 0.00a	1.00 ± 0.00c	6.39 ± 1.29ab	89.59 ± 0.74a
1	90.43 ± 0.76a	−0.50 ± 0.18b	1.86 ± 0.66b	5.93 ± 1.26b	90.21 ± 0.83a
2	90.14 ± 0.53ab	−0.57 ± 0.15b	1.71 ± 0.47b	6.13 ± 1.30b	89.95 ± 0.60a
3	89.14 ± 1.41c	−0.58 ± 0.21b	2.71 ± 0.61a	7.39 ± 1.66a	88.79 ± 1.45b

Means within each column with same letters are not significantly different ($P < 0.05$).
Data are mean ± SD.

Table 3

Mechanical properties of kefir and kefir/NC composites.

Nanocellulose content (%)	Tensile strength (MPa)	Elongation at break (%)	Tensile energy to break (MJ/m ³)	Young's modulus (MPa)
0	6.40 ± 2.62a	18.35 ± 3.76d	19.77 ± 7.83c	382.16 ± 49.05a
1	8.14 ± 1.27a	252.17 ± 27.66a	134.03 ± 35.82a	209.80 ± 50.67b
2	6.41 ± 0.14a	203.66 ± 4.91b	80.46 ± 12.35b	135.84 ± 21.33c
3	5.83 ± 0.30a	168.80 ± 10.10c	63.27 ± 12.95b	70.19 ± 5.40c

Means within each column with same letters are not significantly different ($P < 0.05$).
Data are mean ± SD.

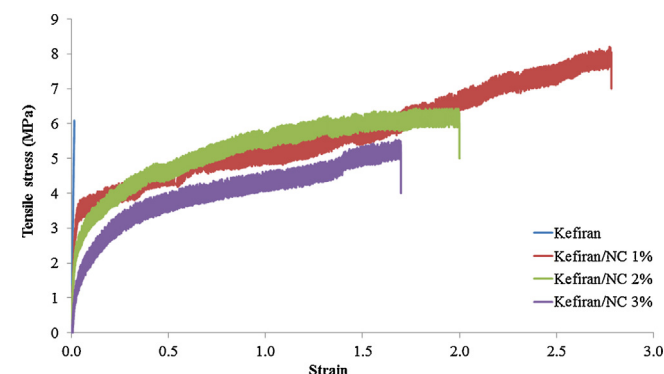
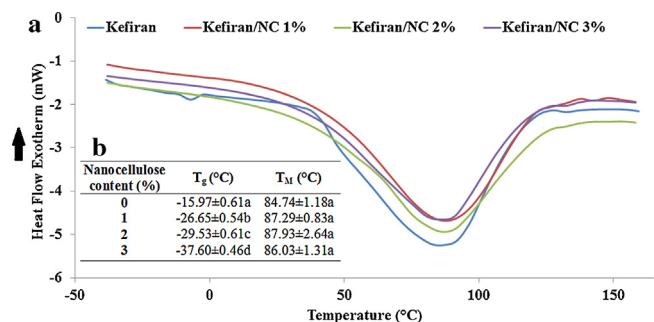
the TS value. These results have been observed in the previous study [27,28]. An adequate distribution of NC in polymer matrix and a good interfacial adhesion between filler and matrix improved mechanical properties of NC based bionanocomposites [19,27,28].

The EB values of kefir/NC composites were at least nine times higher than those of kefir film specimens (Table 3). Kefir/1% NC composite showed maximum EB value. There are a few inconsistencies in the previous studies. Some of the researchers showed that NC decrease EB in the nanocomposites [29], whereas in the other studies, high NC content increased EB of the nanocomposites [27,28]. Bondeson and Oksman showed that NC, as nanofiller, not only decreased TS but also decreased EB [30]. Besides, our previous study showed that some of spherical nanoparticles increased slipperiness of kefir chain and increased EB [2]. Furthermore, it seems produced mono and disaccharides during NC preparation increased EB of the kefir/NCs by plasticizing properties.

The TEB values of all kefir/NC composites were significantly higher than that of kefir film (Table 3). It seems the coagulation of NC in high NC content (2% and 3%) decreased the TEB of nanocomposites.

The YM values of the kefir/NC composites were significantly lower than that of kefir film (Table 3). The YM of the film specimens decreased with increasing NC content. Decreasing YM of the kefir/NC agree with the plasticizing properties of the mono and disaccharide residues in NC.

The mechanical properties of NC based nanocomposites depended on cellulose source, preparation method of NC, and NC content in polymer matrix.

**Fig. 4.** Stress vs. strain for kefir films as a function of NC content.**Fig. 5.** (a) Thermogram and thermal properties of kefir film and kefir/NC composites. (b) Means within each column with same letters are not significantly different ($P < 0.05$); data are mean ± SD.

4.3. Thermal properties

Thermogram and thermal properties of kefir and kefir/NC composites are shown in Fig. 5. The T_g value of kefir/NC specimens decreased drastically after increasing NC content. Soykeabkaew et al. showed bacterial cellulose nanofibers, as a polymer nanofiller, increased T_g of the nanocomposite drastically [27]. In contrast, other researchers showed that T_g of the nanocomposites was independent of NC content [11,30]. These research teams confirmed, the adverse effect of NC on T_g values [11,30]. The dispersion of NC in polymer matrix, hydrogen bonding, and interaction of polymer matrix and NC were mentioned as effective parameter on T_g of the nanocomposites [11,27,30]. Our previous study showed that the flexibility of kefir chains increased by ovalar to whisker shape nano zinc oxide. Perhaps the phenomenon brings about decreasing T_g of the kefir nanocomposites [2]. Furthermore, it seems T_g of the NC composite is dependent on cellulose source, preparation method of NC, and polymer type.

5. Conclusions

According to the results of current study, kefir/NC is an eco-friendly bionanocomposite for food packaging. The EB, TEB, WVP, and visual properties (ΔE) – which are crucial parameters in food packaging – were improved significantly by increasing NC content in the nanocomposites. Furthermore, decreasing YM of kefir/NC nanocomposites with increasing NC content confirmed improving the flexibility of kefir/NC nanocomposites compared to kefir. But, thermal properties, specially T_g , and resistance to water

decreased drastically. On the other hand, T_m was constant. These results were attributed to ball bearing effect of NC in kefir.

Acknowledgements

The authors are grateful to the University of Tehran and Iranian Nanotechnology Initiative Council for providing financial support for this research. We also appreciate the help of Mahar Fan Abzar Co. for the preparation of AFM micrographs.

References

- [1] M. Zolfi, F. Khodaiyan, M. Mousavi, M. Hashemi, *Int. J. Biol. Macromol.* 65 (2014) 340–345.
- [2] I. Shahabi-Ghahfarrokhi, F. Khodaiyan, M. Mousavi, H. Yousefi, *Int. J. Biol. Macromol.* 72 (2015) 41–46.
- [3] J.A. Piermaria, A. Pinotti, M.A. Garcia, A.G. Abraham, *Food Hydrocoll.* 23 (2009) 684–690.
- [4] M. Ghasemlou, F. Khodaiyan, A. Oromiehie, M.S. Yarmand, *Food Chem.* 127 (2011) 1496–1502.
- [5] A.A. Motedayen, F. Khodaiyan, E. Atai Salehi, *Food Chem.* 136 (2013) 1231–1238.
- [6] Z.B. Guzel-Seyd, T. Kok-Tas, A.K. Greene, *Crit. Rev. Food Sci.* 51 (2011) 261–268.
- [7] I. Shahabi-Ghahfarrokhi, F. Khodaiyan, M. Mousavi, H. Yousefi, *Int. J. Biol. Macromol.* 74 (2015) 343–350.
- [8] H. Almasi, B. Ghanbarzadeh, A.A. Entezami, *Int. J. Biol. Macromol.* 46 (2010) 1–5.
- [9] M. Zolfi, F. Khodaiyan, M. Mousavi, M. Hashemi, *Carbohydr. Polym.* 109 (2014) 118–125.
- [10] R.A. Yokel, R.C. MacPhail, *J. Occup. Med. Toxicol.* 6 (2011) 1–27.
- [11] M. Roohani, Y. Habibi, N.M. Belgacem, G. Ebrahim, A.N. Karimi, A. Dufresne, *Eur. Polym. J.* 44 (2008) 2489–2498.
- [12] H. Abdul Khalil, A.H. Bhat, A.F. Ireana Yusra, *Carbohydr. Polym.* 87 (2012) 963–979.
- [13] I. Shahabi-Ghahfarrokhi, F. Khodaiyan, M. Mousavi, H. Yousefi, *Fiber Polym.* 16 (2015) 529–536.
- [14] S.S. Nielsen, in: S.S. Nielsen (Ed.), *Food Analysis Laboratory Manual*, 2nd ed., Springer, New York, 2010, pp. 47–53.
- [15] ASTM, *Annual Book of ASTM*, American Society for Testing and Materials, Philadelphia, 1995, E96–95.
- [16] A. Gennadios, C.L. Weller, C.H. Gooding, *J. Food Eng.* 21 (1994) 395–409.
- [17] ASTM, *Annual Book of ASTM*, American Society for Testing and Materials, Philadelphia, 2002, D882–02.
- [18] ASTM, *Annual Book of ASTM*, American Society for Testing and Materials, Philadelphia, 2004, D3418–03.
- [19] A. Kaushik, M. Singh, G. Verma, *Carbohydr. Polym.* 82 (2010) 337–345.
- [20] E. Tang, C. Cheng, X. Ma, X. Xiaolu, Q. Zhao, *Appl. Surf. Sci.* 252 (2006) 5227–5232.
- [21] A. Kaushik, M. Singh, *Carbohydr. Res.* 346 (2011) 76–85.
- [22] A. Alemdar, M. Sain, *Bioresour. Technol.* 99 (2008) 1664–1671.
- [23] M. Fan, D. Dai, B. Huang, in: S.M. Salih (Ed.), *Fourier Transform – Material Analysis*, In Tech, 2012, pp. 45–68.
- [24] B. Stuart, *Infrared Spectroscopy: Fundamentals and Applications*, John Wiley & Sons, 2004, pp. 45–93.
- [25] J. Piermaria, A. Bosch, A. Pinotti, O. Yantorno, M.A. Garcia, A.G. Abraham, *Food Hydrocoll.* 25 (2011) 1261–1269.
- [26] C.J. Grande, F.G. Torres, C.M. Gomez, O.P. Troncoso, J. Canet-Ferrer, J. Martínez-Pastor, *Mater. Sci. Eng. C* 29 (2009) 1098–1104.
- [27] N. Soykeabkaew, N. Laosat, A. Ngaokla, N. Yodsuwan, T. Tunkasiri, *Compos. Sci. Technol.* 72 (2012) 845–852.
- [28] N.R. Savadekar, S.T. Mhaske, *Carbohydr. Polym.* 89 (2012) 146–151.
- [29] M. Hietala, A.P. Mathew, K. Oksman, *Eur. Polym. J.* 49 (2013) 950–956.
- [30] D. Bondeson, K. Oksman, *Compos. Part A* 38 (2007) 2486–2492.